

Enhanced coercivity in thermally processed (Nd,Dy)(Fe,Co,Nb,B)_{5.5}/α-Fe nanoscale multilayer magnets

W. Liu^{a)}

Shenyang National Laboratory for Materials Science, Institute of Metal Research, and International Centre for Materials Physics, Chinese Academy of Science, Shenyang 110016, People's Republic of China

X. Z. Li

Center for Materials Research and Analysis, University of Nebraska, Lincoln, Nebraska 68588

J. P. Liu

Department of Physics, University of Texas at Arlington, Arlington, Texas 76019

X. K. Sun and C. L. Chen

Shenyang National Laboratory for Materials Science, Institute of Metal Research, and International Centre for Materials Physics, Chinese Academy of Science, Shenyang 110016, People's Republic of China

R. Skomski

Center for Materials Research and Analysis, University of Nebraska, Lincoln, Nebraska 68588

Z. D. Zhang

Shenyang National Laboratory for Materials Science, Institute of Metal Research, and International Centre for Materials Physics, Chinese Academy of Science, Shenyang 110016, People's Republic of China

D. J. Sellmyer

Center for Materials Research and Analysis, University of Nebraska, Lincoln, Nebraska 68588

(Received 12 November 2004; accepted 11 March 2005; published online 3 May 2005)

Structural and magnetic properties of laminated (Nd,Dy)(Fe,Co,Nb,B)_{5.5}/Fe nanocomposites are investigated. Normally, the addition of the soft phase to the hard phase enhances the remanence but deteriorates the permanent-magnet performance of the material by reducing the coercivity. In the present system, the coercivity *increases* to 1608 kA/m (20.2 kOe) in thermally processed Nd–Dy–Fe–Co–Nb–B(15 nm)/Fe(4 nm) multilayered nanocomposites, which is higher than that of the single-layer hard-magnetic film. The abnormally high coercivity is achieved by annealing at relatively high temperature, which breaks the laminated structure of the as-deposited multilayer. A likely physical explanation of the enhanced coercivity is the introduction of the domain-wall pinning sites that counteract the inevitable decrease of the nucleation field. © 2005 American Institute of Physics. [DOI: 10.1063/1.1905788]

I. INTRODUCTION

For more than one decade, extensive experimental and theoretical research has been done on exchange-coupled hard-soft^{1–14} permanent magnets. However, up to now, experimentally achieved energy products have been lower than the theoretical limit predicted for optimized² nanocomposite magnets. The idea of hard-soft nanostructuring is to exploit the high saturation magnetization of the soft phase while minimizing the sacrifice of coercivity. In practice, the latter requirement, namely the control of the coercivity by developing a suitable nanostructure, is the key consideration.^{5–13} Examples are nanostructured Co–Sm/Fe–Co and Pr–Co/Co multilayers prepared by sputtering and subsequent heat treatment,^{9,10} exchange-coupled α-Fe/Nd–Fe–B multilayer magnets as investigated by Shindo *et al.*¹¹ the Nd–Fe–B/Fe/Nd–Fe–B trilayers reported by Parhofer *et al.*¹² and Yang and Kim,¹³ NdFeB/Co films reported by O'Shea and Cui,¹⁴ and our (Nd,Dy)(Fe,Co,Nb,B)_{5.5}/α-Fe

multilayer films,¹⁵ which exhibit a high maximum energy product of $(BH)_{\max} = 203 \text{ kJ/m}^3$ (25.6 MGOe).

Typically, multilayering with iron tends to reduce the coercivity of Nd–Fe–B thin films¹¹ because the soft iron reduces the nucleation field.² In the present paper, a remarkably high coercivity is reported for nanocomposite (Nd,Dy)(Fe,Co,Nb,B)_{5.5}/α-Fe multilayer films deposited on a silicon substrate. The stoichiometry and fabrication of the present films are different from previously investigated systems.^{11–14}

II. EXPERIMENT

To prepare the (Nd,Dy)(Fe,Co,Nb,B)_{5.5}/α-Fe thin films, a multiple-gun dc- and rf-sputtering system was used. The iron and (Nd_{0.9}Dy_{0.1})(Fe_{0.77}Co_{0.12}Nb_{0.03}B_{0.08})_{5.5} targets were deposited onto silicon substrates covered with a 20-nm Ti buffer. The alloy target was made by sintering powdered ingots and others (Fe and Ti) were commercial products. The purities of the metal targets were all higher than 99.9%. The base pressure of the sputtering system was $(2–3) \times 10^{-7}$ Torr, the Ar pressure was 5 mTorr during the sputtering, and the substrates were held at room temperature.

^{a)}Author to whom correspondence should be addressed; FAX: 86-24-23893120; electronic mail: wliu@imr.ac.cn

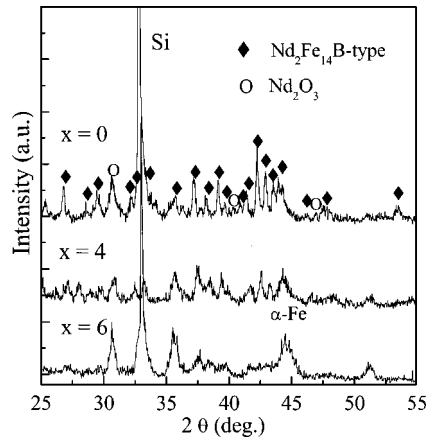


FIG. 1. XRD patterns for the Ti(20 nm)/[Nd–Dy–Fe–Co–Nb–B(15 nm)Fe(x nm)] \times 20/Ti(20 nm)/(Si substrate) multilayer annealed at 625 °C for 1 min.

The film thickness was measured by weighing the mass of the films. The as-deposited films were then heat treated in a furnace with a vacuum of 2×10^{-7} Torr. They have the structure Ti(20 nm)/[Nd–Dy–Fe–Co–Nb–B(15 nm)Fe(x)] \times 20/Ti(20 nm)/(Si substrate), where $x=0$ –10 nm.

The crystalline structure of the phases in the films was determined by x-ray diffraction (XRD) with Cu $K\alpha$ radiation, and the nanostructure was studied by transmission electron microscopy (TEM) and high-resolution transmission electron microscopy (HRTEM). The magnetic properties of the films were measured by an alternating gradient-force magnetometer (AGFM) and a superconducting quantum interference device (SQUID) magnetometer.

III. RESULTS AND DISCUSSION

Figure 1 shows the XRD patterns for the Ti(20 nm)/[Nd–Dy–Fe–Co–Nb–B(15 nm)Fe(x)] \times 20/Ti(20 nm)/(Si substrate) multilayer annealed at 625 °C for 1 min. The as-deposited single-layer film ($x=0$) is amorphous. For the Nd–Dy–Fe–Co–Nb–B/ α -Fe multilayer, the amorphous Nd–Dy–Fe–Co–Nb–B and α -Fe are observed in the as-deposited multilayer, in agreement with the TEM result in Ref. 15. After being annealed at 625 °C for 1 min, a Nd₂Fe₁₄B-type hard-magnetic phase forms, accompanied by a trace of Nd₂O₃. In all annealed films, the Nd₂Fe₁₄B-type phase is randomly oriented.

Figure 2 shows room-temperature hysteresis loops for different iron-layer thicknesses x after annealing at 625 °C for 1 min. Figure 3 shows the remanence and the coercivity of the films for different Fe-layer thicknesses and annealing conditions. The remanence tends to increase with x , indicating that the Fe and 2:14:1 regions are exchange coupled. The coercivity exhibits the maximum at $x=4$ nm, in contrast to the normally encountered monotonous decrease. The coercivity at $x=4$ nm, 1608 kA/m (20.2 kOe), is significantly higher than that of the single layer ($H_c=1353$ kA/m, or 17.0 kOe). The unusual coercivity increase is observed for all three annealing regimes shown in Fig. 3. We therefore conclude that short-time annealing of suitable-multilayered

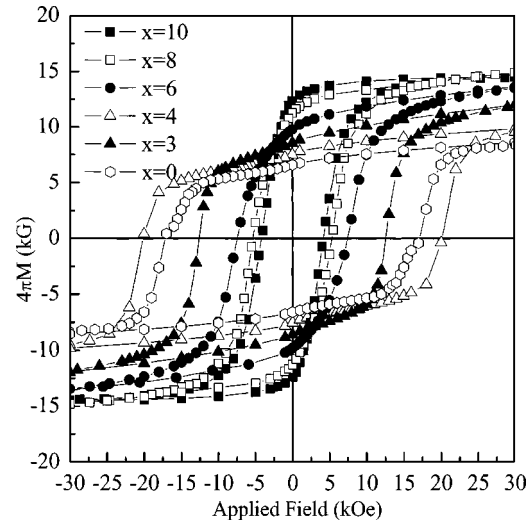


FIG. 2. Room-temperature hysteresis loops of the Ti(20 nm)/[Nd–Dy–Fe–Co–Nb–B(15 nm)Fe(x nm)] \times 20/Ti(20 nm)/(Si substrate) multilayer annealed at 625 °C for 1 min. The magnetization is plotted as a function of the external field, that is, without the demagnetizing-field corrections.

nanostructures can be used to improve the coercivity while keeping the remanence above that of films without iron layers.

To study the origin of the coercivity enhancement, we have investigated the microstructure of the films with $x=4$ nm by TEM and high-resolution electron microscopy (HREM). Figure 4 shows the TEM bright-field image of the film annealed at 625 °C for 1 min, where (a) is a cross-section TEM image of the multilayer film and (b) is a HREM image of the grains in the multilayer film. As shown earlier,¹⁵ the distribution of the as-deposited soft- and hard-phase layers in the multilayer films is very uniform. (In the cross-section view in Ref. 15, the amorphous Nd–Dy–Fe–Co–Nb–B and Fe layers are clearly visible.) However, the cross-section view of Fig. 4(a) shows that the laminated structure of the as-deposited multilayer film has been broken com-

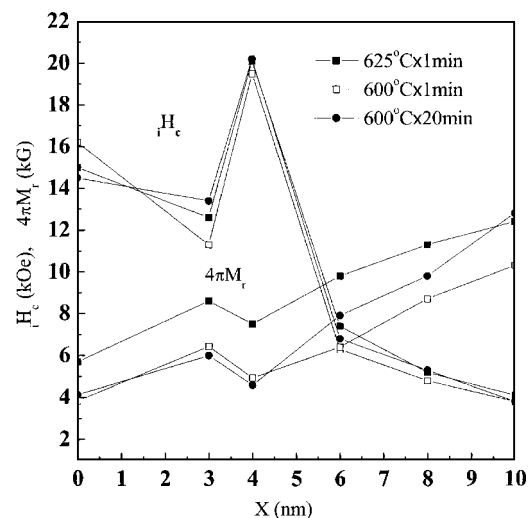


FIG. 3. The remanence and coercivity of Ti(20 nm)/[Nd–Dy–Fe–Co–Nb–B(15 nm)Fe(x nm)] \times 20/Ti(20 nm)/(Si substrate) as a function of the thickness x of the Fe layers for different annealing conditions.

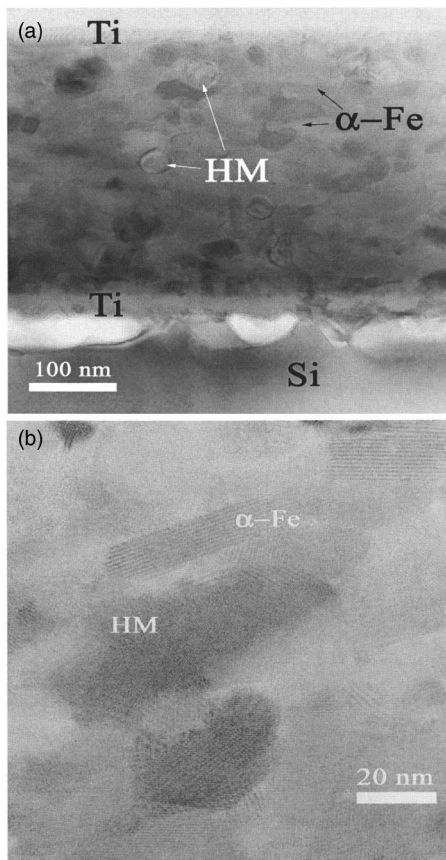


FIG. 4. The microstructure of the $x=4$ nm film annealed at $625\text{ }^{\circ}\text{C}$ for 1 min: (a) a cross-section TEM image of the multilayer film and (b) HREM image of the grains in the multilayer film.

pletely by annealing for only 1 min. This reflects the higher annealing temperature as compared to Ref. 15.

Figure 4(a) shows the grain morphology and distribution of the hard-magnetic phase with a grain size of about 40 nm and the soft-magnetic $\alpha\text{-Fe}$ phase with irregular shape. Figure 4(b) reveals a clear grain boundary between the hard grains, and the shape of the hard grains is aspherical. The soft regions have a nearly rectangular shape, dimensions close to $10 \times 50\text{ nm}^2$, and are well distributed and embedded in the hard phase.

To analyze the enhanced coercivity of the films with $x=4$ nm, it is instructive to compare Fig. 4 with the microstructure observed for other thicknesses. Figure 5 shows a cross-section TEM for a film with $x=6$ nm, annealed at $625\text{ }^{\circ}\text{C}$ for 1 min. It is seen that the laminated structure consisting of the soft- and hard-magnetic components survives in the multilayer. In comparison with the result in Fig. 4, it is found that although the heat treatment condition was the same for these two cases, the annealing could not break the laminated structure of the as-deposited multilayer for the Fe thickness up to 6 nm (see Ref. 15), similar to our previous work.¹⁶ From the result of XRD patterns (see Fig. 1), the hard phase 2:14:1 has been well formed with the soft phase of $\alpha\text{-Fe}$ in multiplayer. Although the final nanostructure of the multilayer film is not ideal, the laminated nanostructure consisting of mutually dispersed soft and hard phases can still result in the enhancement of the remanent magnetiza-

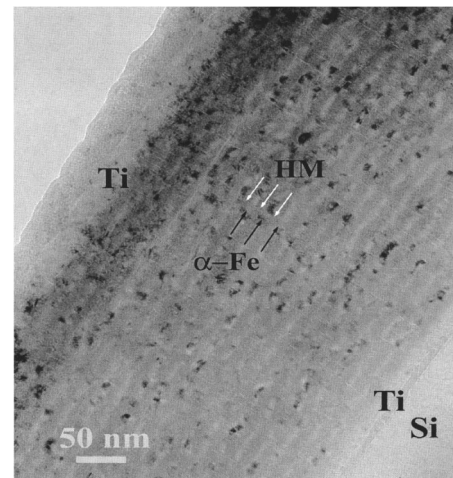


FIG. 5. The cross-section TEM image of the film with $x=6$ nm, annealed at $625\text{ }^{\circ}\text{C}$ for 1 min.

tion. Such a nanostructure leads to the obvious decrease of coercivity in comparison with the result of the multilayer for $x=4$.

In most cases, the intrinsic coercivity H_c of the nanocomposite permanent magnets *decreases* with increasing volume of the soft phase. There are two reasons. First, there is a decrease in the effective anisotropy constant $K_{\text{eff}} = f_s K_s + f_h K_h$, where f_s , f_h and K_s , K_h represent the volume fractions and anisotropy constants of the soft and hard components, respectively.^{2,8} Second, adding a soft phase tends to enhance the average size of the soft regions, which leads to a reduction of the nucleation field.^{2,17} Generally in coarser structures, the coercivity is smaller than predicted from K_{eff} .² Going from $x=0$ to $x=4$ nm, the reduction of the volume fraction f_h of the hard phase from 1.0 ($x=0$) to 0.79 ($x=4$) corresponds to a reduction of K_{eff} by 21%. Estimating H_c from the anisotropy field, $H_a = 2K_{\text{eff}} / \langle M_s \rangle$, yields the conservative prediction of a coercivity reduction by 27%, in striking contrast to the experimental coercivity increases from 14.5 kOe ($x=0$) to 20.2 kOe ($x=4$) for the films annealed at $625\text{ }^{\circ}\text{C}$ for 1 min.

A likely explanation for the anomaly is that annealing creates pinning centers at the interfaces between the hard and soft layers, which may effectively impede the movements of the domain during magnetization reversal. In the as-deposited film, the interfaces are relatively clean, and domain walls can move relatively easily. After annealing, the contaminated interfaces exist in the boundaries of the hard and soft phases due to their interdiffusion, and the resulting imperfections act as pinning centers that enhance the coercivity. Especially, it should be noted that pinning is most effective on a size scale of pinning regions comparable to the effective domain-wall width determined by K_{eff} , i.e., $\sim 5\text{ nm}$.¹⁷ For too large or too small size of pinning regions, the pinning is less effective, and the above-mentioned coercivity-reduction mechanisms take over. When $x < 4$, the quantity and size scale of the pinning centers from the contaminated interfaces is small, so the coercivity of the films *decreases* with increasing volume of the soft phase. For the case $x=4$, annealing likely provides a microstructure satisfy-

ing the condition of most effective pinning, because a suitably large amount of effective pinning centers with comparable size scale to the effective domain-wall width enhances the coercivity. On the other hand, the reduction of the remanence for $x=4$ as seen from Fig. 3 implies the decrease of the effective exchange coupling between the hard and soft phases, due to interface contamination or imperfections. For $x \geq 6$, a clear-layered structure is observed as shown in Fig. 5. It implies that the pinning centers to enhanced coercivity are not noticeably formed.

IV. CONCLUSIONS

We have used sputtering to prepare multilayer films consisting of hard $\text{Nd}_2\text{Fe}_{14}\text{B}$ -type and soft α -Fe phases. Subsequent heat treatment yields an anomalous increase of the coercivity when the thickness of the soft layers is equal to 4 nm. The coercivity enhancement is of practical importance because the usually encountered coercivity decreases on adding iron is a serious limitation to energy-product development in hard-soft nanostructures. The coercivity-enhanced films differ from the as-deposited films and from films with thick iron layers by the absence of a laminated structure. A likely explanation of the coercivity maximum is the domain-wall pinning due to nanostructure changes.

ACKNOWLEDGMENTS

This work has been supported by the U.S. NSF under Grant No. INT-9812082, NSF MRSEC, the U.S. DOE, the

National Natural Science Foundation of China under Projects Nos. 50331030 and 50371085, and by the National 863 project under Grant No. 2002AA302603.

- ¹R. Coehoorn, D. B. de Mooij, and C. D. E. Waard, *J. Magn. Magn. Mater.* **80**, 101 (1989).
- ²R. Skomski and J. M. D. Coey, *Phys. Rev. B* **48**, 15812 (1993).
- ³T. Schrefl, H. Kronmüller, and J. Fidler, *J. Magn. Magn. Mater.* **127**, L237 (1993).
- ⁴E. F. Kneller and R. Hawig, *IEEE Trans. Magn.* **27**, 3588 (1991).
- ⁵J. Ding, P. G. McCormick, and R. Street, *J. Magn. Magn. Mater.* **124**, 1 (1993).
- ⁶A. Manaf, R. A. Buckley, and H. A. Davies, *J. Magn. Magn. Mater.* **128**, 302 (1993).
- ⁷L. Withanawasam, A. S. Murphy, G. C. Hadjipanayis, and R. F. Krause, *J. Appl. Phys.* **76**, 7065 (1994).
- ⁸X. K. Sun, J. Zhang, Y. L. Chu, W. Liu, B. Z. Cui, and Z. D. Zhang, *Appl. Phys. Lett.* **74**, 1740 (1999).
- ⁹I. A. Al-Omari and D. J. Sellmyer, *Phys. Rev. B* **52**, 3441 (1995).
- ¹⁰J. P. Liu, Y. Liu, R. Skomski, and D. J. Sellmyer, *IEEE Trans. Magn.* **35**, 3241 (1999).
- ¹¹M. Shindo, M. Ishizone, A. Sakuma, H. Kato, and T. Miyazaki, *J. Appl. Phys.* **81**, 4444 (1997).
- ¹²S. Parhofer, J. Wecker, C. Kuhrt, and G. Gieres, *IEEE Trans. Magn.* **32**, 4437 (1996).
- ¹³C. J. Yang and S. W. Kim, *J. Magn. Magn. Mater.* **202**, 311 (1999).
- ¹⁴M. J. O'Shea and B. Z. Cui, *IEEE Trans. Magn.* **40**, 2889 (2004).
- ¹⁵W. Liu, Z. D. Zhang, J. P. Liu, L. J. Chen, L. L. He, Y. Liu, X. K. Sun, and D. J. Sellmyer, *Adv. Mater. (Weinheim, Ger.)* **14**, 1832 (2002).
- ¹⁶W. Liu, Z. D. Zhang, J. P. Liu, Z. R. Dai, Z. L. Wang, X. K. Sun, and D. J. Sellmyer, *J. Phys. D* **36**, L63 (2003).
- ¹⁷R. Skomski, *J. Phys.: Condens. Matter* **15**, R841 (2003).